



Expanding up to far-infrared filamentation-induced supercontinuum spanning in chalcogenide glasses

O. Mouawad^{1,2} · P. Béjot¹ · P. Mathey¹ · P. Froidevaux¹ · A. Lemièrè¹ · F. Billard¹ · B. Kibler¹ · F. Désévéday¹ · G. Gadret¹ · J.-C. Jules¹ · O. Faucher¹ · F. Smektala¹

Received: 3 January 2018 / Accepted: 1 August 2018 / Published online: 24 August 2018
© Springer-Verlag GmbH Germany, part of Springer Nature 2018

Abstract

We report on far-infrared filament-induced supercontinuum obtained with three chalcogenide glasses. The introduction of more polarizable elements (Se instead of S and Te instead of S and Se) into the glasses increases their non-linearity and transmission window and also shifts gradually corresponding zero-dispersion wavelength in the infrared region. Overall chalcogenide glasses were pumped with 65-fs pulses at the optimal wavelength with respect to supercontinuum extension. An infrared spanning reaching the 16- μm threshold is obtained.

1 Introduction

The technology of ultrafast lasers has developed over the second half of the last century. The modern optics was marked by the great contribution of femtosecond sources, especially for supercontinuum generation (SCG). The propagation of intense ultrashort pulses in bulk non-linear medium promotes particular phenomena termed femtosecond filamentation, yielding to a spectral broadening, commonly known as SCG. The first experimental recording of such spectral expansion was reported in bulk borosilicate glass [1]. Ever since, extended multidisciplinary studies were conducted about the interaction between the dielectric transparent material and the intense ultrashort pulse at the origin of the filamentation. This phenomenon reported in a wide variety of transparent materials [2] was found to be the result of several non-linear phenomena (Kerr self-focusing and generation of free carriers) [3–6]. In this context, the advantageous mid-infrared (MIR) transmitting and non-linear chalcogenide glasses (ChGs) have stimulated the interest of the scientific community. This quest is mainly

promoted by the mid-IR wavelength regime which is of particular importance to chemical, medical, and environmental sciences, as it covers the fundamental vibrational absorption bands of polar molecules and of many gaseous molecules, biomolecules, solid state compounds, etc.

ChGs are optical materials that are transparent in the infrared range extended between 2 and 25 μm [7–9]. These inorganic vitreous materials contain one or several chalcogen elements (S, Se, and Te) with other elements such as As, Ge, and Ga, which exhibit a higher electropositivity compared to chalcogen. In addition, due to the high atomic weight of chalcogen elements, the phonon energy of ChGs is low (350–200 cm^{-1}). Besides, both linear refractive index (> 2) and optical non-linearity (~ 2 – 3 orders greater than that of silica) are considerably high. These last properties might be significantly tailored upon controlling the composition of the glass. In general, optical non-linearity is directly proportional to the weight of the chalcogen element present in the glass sample [10]. A wide range of applications, especially the SCG, may benefit from these features. These features promote ChGs as materials of primary choice for developing devices [4, 5] for widespread optical applications in IR imaging, IR lasers, chemical sensing, and optical communication [11–14]. Among the various ChG systems, most attention was dedicated to glasses based on chalcogenides of arsenic and antimony, including several binary as well as ternary materials As–S(Se), As–Sb–S(Se), Ge–As–S(Se), Ge–Sb–S(Se), and As–Te–Se [15, 16]. Despite the interesting results reported on these glass systems, the toxic aspect of As and Sb could limit their prospective applications,

✉ F. Smektala
frederic.smektala@u-bourgogne.fr

¹ ICB, Laboratoire Interdisciplinaire Carnot de Bourgogne, UMR 6303 CNRS-Université de Bourgogne Franche-Comté, 9 Av. Alain Savary, BP 47870, 21078 Dijon, France

² Laboratoire Énergétique et Réactivité à l'Echelle Nanométrique (EREN), Université Libanaise FSIV, Haouch El-Omara, Zahleh 1801, Lebanon

especially in the environmental, biological, and medicinal fields. For this reason, different studies have been carried out in the last few years with the aim to remove As and Sb [17–23].

Besides submitted effort conducted to develop As- and Sb-free ChG-based optical glasses, scientific community continues to explore the MIR SCG in different materials in both fibers [22–27] and bulk [28–30] form, without succeeding to cover entire transparency window of the investigated materials. Nevertheless, the most promising experimental results were registered in bulk materials involving self-focused filaments. In both cases, the pump source was usually an optical parametric amplifier (OPA), to ensure the optimal pumping regime, in terms of pump wavelength and pump power.

In this study, we investigate As- and Sb-free ChGs consisting of stable compositions of Ge–S–Se, Ge–Se, and Te–Ge–Ga families for MIR SCG purposes. Pumping several millimeters of each glass using an OPA with 65 fs pulses and a convenient average power at the pump wavelength, we generate a spectral broadening covering an extended range of the corresponding transmission window.

2 Experiments

2.1 Glass synthesis

Bulk glasses in 15-g batches were prepared by the melt-quenching technique [17, 26]. Elemental raw materials (Ge, S, Se, and Te 5N) of analytical quality were weighed according to the predefined stoichiometry $\text{Ge}_{23.8}\text{S}_{57.1}\text{Se}_{19.1}$ (GSSe), GeSe_4 (GeSe), and $\text{Te}_{75}\text{Ge}_{15}\text{Ga}_{10}$ (TGG). They were introduced into silica ampoules previously cleaned using an HF solution. To get rid of moisture from the inner surface of silica ampoules and that of starting materials gathered inside, a high secondary vacuum (10^{-9} bar) was established for 24 h inside the setup. The resultant sealed ampoules were thereafter introduced into a rocking tubular furnace and heated up to the formation temperature, respective of each composition (between 700 and 900 °C), for a period of 12 h to ensure a complete reaction. At the end of this step, each molten bath enclosed inside a silica ampoule was suddenly cooled in a water bath, and the glass was obtained. To relieve the mechanical stress resulting from quenching, the samples were annealed by heating at 10 °C below the glass transition temperature (T_g), for a period of 5 h, before being gradually cooled down to the ambient temperature according to a suitable time–temperature program. Glass rods were obtained at the end of this stage. Diamond saws were used to cut the rods into discs several millimeters' thick. These were polished to reflect the softness of both sides using SiC paper and diamond suspensions (3–0.5 μm).

2.2 Optical characterization of the glass plates

The glass transmission spectra for wavelengths from the near infrared to the MIR (1.7–25- μm range) were measured with a Bruker IFS 28 Spectrophotometer. Measurements were performed on samples of few millimeters' thicknesses (mentioned in Fig. 1a–c). The corresponding transmission spectra are plotted in Fig. 1. They show a transmission in the 2–11-, 2–17-, and 2–22- μm ranges for GeSSe, GeSe, and TGG, respectively.

The IR cut-off wavelength reflecting the multiphonon absorption (Fig. 1) follows the trend predicted by Hooke's law. As expected, spectra long-wavelength edges shift to the MIR upon increasing the atomic mass of chalcogenide element ($_{16}\text{S}$, $_{34}\text{Se}$, and $_{52}\text{Te}$, respectively). Apart from the materials' intrinsic absorptions (bandgap and multiphonon), the transmission window was found to be interrupted by several absorption peaks. Since the glasses were not further purified, such impurities are more likely in high concentration. In addition, oxides impurities were found to be the main impurities contributing to these absorptions. The set of the main absorption peaks interrupting the glass transmission is presented in Fig. 1. Peak assignments were based on the published literature on various systems [10, 31–34] due to the oxygen pollution of the glass. Strong absorptions attributed to Ge–O bonds arise around 8, 12, and 15 μm . In addition, the optical transmission of TGG glass shows a broad absorption in the 14–20- μm region, also due to oxygen impurities. These absorptions become crucial for long samples such as optical fibers and narrow the operational transmission window.

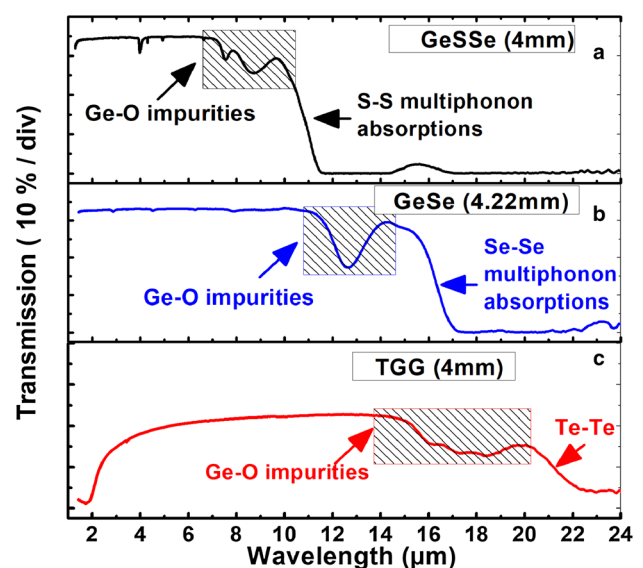


Fig. 1 Optical transmission of the investigated non-purified glasses

2.3 Setup for non-linear optical measurements

Figure 2 shows schematically the experimental setup used to generate the continuum spectra reported in this work. The experiment is performed using a commercial non-collinear optical parametric amplifier (NOPA) (Topas-Prime, Light Conversion Ltd.), pumped by an amplified Ti:sapphire laser system (Spitfire-PRO, Newport-Spectra Physics). The Ti:sapphire system delivers pulses centered at 790 nm with 3-mJ energy per pulse (100 fs pulse duration) at 1-kHz repetition rate. About 300-μJ, 65-fs near-infrared pulses (between 1.1 and 2.6 μm) are generated by directing the beam to the NOPA. The beam diameter at the output of the NOPA is approximately 1 cm (at $1/e^2$) and the spatial mode quality factor (M^2) is less than 1.3. To separate the signal beam (horizontally polarized) from the idler beam (vertically polarized), an LP-1500-nm long-wavelength pass filter and a polarizer are placed after the NOPA. As the non-linear media, we used polished samples of several millimeters' thicknesses of the three chalcogenide glasses GeSSe, GeSe, and TGG. The refractive indices of these glasses are listed in Table 1.

The non-linear refractive index of these glasses is around $15 \times 10^{-18} \text{ m}^2/\text{W}$ [35], and the zero-dispersion wavelength (ZDW) is located close to 6.4 μm (resp. 6.5 μm) for GSSE (resp. GeSe) glass. Glass samples are fixed on a home-made translation stage, and the incident beam is focused at the entrance face of the sample. The pump wavelength is chosen to belong to the range of maximum broadening efficiency of all three investigated glasses. Broadband measurements are performed with a Newport Cornerstone™ 130 1/8-m motorized monochromator, equipped with two diffraction gratings adapted for the wavelength range of interest. The first grating is operational in the 1.1–5.0-μm range. It has a 300-l/mm line density and a peak efficiency of 90% at the 405-nm blaze wavelength, providing a spectral resolution of 5 nm. The second grating is operational in the 4.5–22-μm

range. It has a 150-l/mm line density and a peak efficiency of 75% at the 6000-nm blaze wavelength.

The beam entering the monochromator is focused on the input slit using a Ge lens. The beam at the output of the monochromator is focused on the MCT detector with a CaF₂ lens for GeSSe and GeSe, while a gold-coated concave mirror is employed upon testing TGG specimen. The spectra are recorded from 2 to 16 μm with a liquid-nitrogen cooled MCT detector owing a peak wavelength located around 12 μm with an operating range reaching 16 μm. High-order grating reflections and their inherent overlapping with the continuum spectra are excluded using various germanium long-pass filters. In this context, spectra are registered separately with Ge filters transmitting above 3, 5, 7, 9, and 11 μm and sequentially placed in front of the detector. Finally, the spectra from each acquisition were slightly scaled to be consistent in the overlap region.

3 Results and discussion

3.1 Supercontinuum in GeSe glass (Ge_{23.8}S_{57.1}Se_{19.1})

Figure 3a shows the experimental results achieved by pumping a 4.0-mm-thick sample of GeSSe glass. The optimal pump wavelength was found around 4.5 μm, almost 2 μm far from the materials' ZDW [35], due to the superior experimental conditions mainly related to higher pump power. The energy threshold required for continuum spanning was found around 3 μJ at 1 kHz, equivalent to 46.153-MW peak power ($P = E/\tau$), corresponding to $520P_{cr}$. The corresponding critical peak power (P_{cr}) is ~0.088 MW. Let us recall that upon coupling intense pulse into transparent material, peak power must overcome a threshold (P_{cr}) to initiate self-focusing. It is calculated as $P_{cr} = 3.77\lambda^2/8\pi n_0 n_2$ [37, 38], where λ is the laser

Fig. 2 Schematic representation of the experimental setup

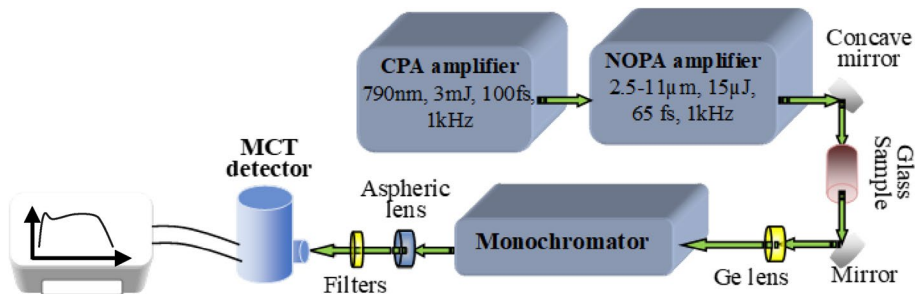


Table 1 Refractive indices of glass samples

Glass sample	GeSSe	GeSe	TGG
Linear refractive index	2.3103 at 2.2 μm [35]	2.4266 at 2.2 μm [35]	3.44 at 3.0 μm [36]

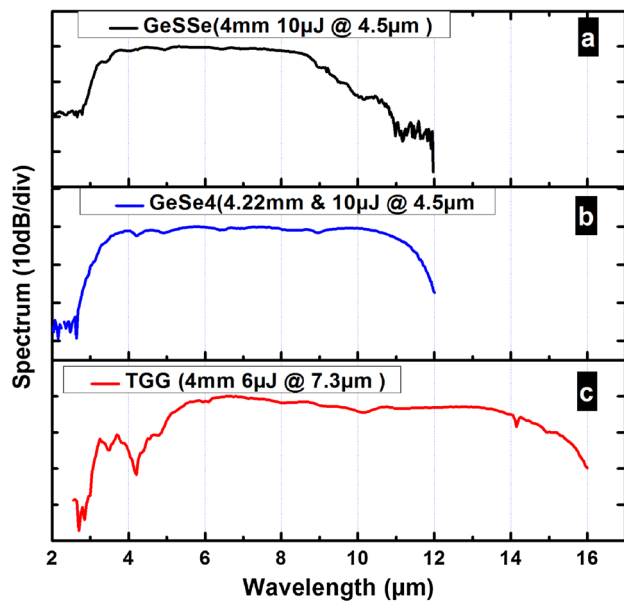


Fig. 3 Spectral measurements carried out on the probed chalcogenide glasses

wavelength, and n_0 and n_2 are the linear and non-linear refractive indices. The maximum spanning is registered here for a peak power almost ~ 1700 times greater than the critical one. The present 10- μJ (153 MW) continuum significantly exceeds the 2 octaves level and is remarkably flat. It spreads over 8.4 μm (from 2.6 to 11 μm) in the -20 -dB range. The spectral range was considered according to the noise level of the detection system. By comparing the continuum registered in GeSSe to that generated in GeSe (see the next paragraph), upon operating in the same conditions (sample dimensions, pump wavelength, and energy), we can distinguish a clear decrease in the spectral broadening. This phenomenon is mainly related to the difference in the glass composition. Substituting S atoms by heavier Se atoms increases the band-gap wavelength, shifts upward the IR transmission wavelength edge, and increases the refractive index as well as the non-linear one. Since the GSSe glass is rich in S, S–S multiphonon occurs, limiting the long-wavelength transmission edge to ~ 12 μm , as it is the case in selenium-free compounds, such as GeS_3 [39]. Besides that, S is more vulnerable than Se to oxide and water pollution. Since no pre-synthesis purification was carried out on the GeSSe sample, more oxide impurities, mainly Ge–O, remain in the glass during the glass synthesis. The corresponding absorption signature appears in the 7–12- μm range [31], significantly reducing the efficiency of the non-linear spectral broadening over this region, as revealed by our SC measurements.

3.2 Supercontinuum in GeSe glass (GeSe_4)

Figure 3b shows the experimental results achieved by pumping a 4.22-mm-thick sample of GeSe glass. As for the previous sample, on site filament formation, experiments were carried out using different pump wavelengths and pulse energies. The required parameters are found to be quite similar to that obtained for GeSSe glass. Again, the optimal pump wavelength was found around 4.5 μm [35]. In addition, the threshold energy for continuum appearance was 3 μJ ($P = E/\tau = 46.153$ MW) at 1 kHz. The critical peak power for filament emergence in GeSe glass is ~ 0.083 MW (calculated using the same equation as above). Consequently, the non-linear response becomes significant when $P \sim 553P_{\text{cr}}$. This response enhances the spectral broadening to reach the maximum spreading upon employing a peak power ~ 1800 times greater than the critical value. As for GeSSe glass, the 10- μJ continuum significantly exceeds the 2 octaves level and is remarkably flat. However, the corresponding spectral range is significantly extended and spreads over 9.4 μm (from 2.6 to 12 μm) in the -20 -dB range. The spectral range was considered according to the noise level of the detection system.

The short wavelength edge of the spectrum has reached the minimum detection limits (around 2.0 μm) of the detection system (grating and MCT detector). However, the long-wavelength edge of the continuum relies in the range of maximum sensitivity of the detector (~ 12 μm). Despite the MCT detector is operational up to 16 μm (high intensity is required, since the sensitivity exponentially decreases), the continuum generated in the GeSe sample did not succeed to overcome the 12- μm limit. This is mainly due to the CaF_2 lens owing a cut-off wavelength located below 12 μm and placed between the monochromator and the MCT detector. Thus, no signal is collected above this critical wavelength. Besides that, other unsuitable phenomena inherent to the glass sample, more precisely the extrinsic absorptions, might be added to the previous one to explain such results. It is known that several extrinsic impurity absorptions contribute to the signal extinction. According to Fig. 1b, the glass transmission is interrupted in the 11–14- μm range, with absorption of almost 50% of the available signal. This is the result of absorptions mainly attributed to Ge–O bonds arising around 8 and 15 μm . Consequently, the intensity of the non-linear phenomenon is strongly reduced upon approaching this absorption, and no further expansion in the infrared region is permitted.

3.3 Supercontinuum in TGG glass ($\text{Te}_7\text{Se}_{15}\text{Ga}_{10}$)

Figure 3c shows the experimental results achieved by pumping a 4-mm-thick sample of TGG glass. Filament formation experiments were carried out using different pump

wavelengths and pulse energies. As expected, the optimal pump wavelength was found around 7.3 μm , next to the materials' ZDW. For that sample, the band-gap wavelength is red-shifted, the maximum transmission is reached at higher wavelength (Fig. 1c), and low wavelength pumping leads to absorptions which are unsuitable for SCG. However, the higher non-linearity of the TGG glass requires lower pumping energy and allows efficient SCG when pumping at higher wavelength close to the ZDW. The threshold energy for filament appearance (as well as supercontinuum) was 1.5 μJ ($P = E/\tau = 23.153 \text{ MW}$) at 1 kHz. The critical peak power for filament emergence is 0.155 MW in TGG glass. Therefore, in our experiment, the observable broadening started to appear at $P \sim 149P_{\text{cr}}$. When the peak power reached $P \sim 149P_{\text{cr}}$, the homogeneous supercontinuum image decreased and multiple patterns—evidence of multiple filament formation—started to appear. The broadest continuum was achieved using peak powers ~ 600 times greater than the critical value. It spans from 2.5 μm up to 16 μm and is characterized by a 13.5- μm bandwidth. The resulting 6- μJ supercontinuum exceeds the 2 octaves level and is remarkably flat (a 13.5- μm span contained in a -20-dB range). Both lower and upper edges of the spectrum have reached the lower detection limits of the detection system (grating and MCT detector) and succeeded to rise up from the noise level of the detection system.

3.4 Some comments about GeSe and TGG pumping

When comparing the results obtained with GeSe and TGG, despite that the dimensions of the glass samples are similar and the energy employed to initiate the non-linear response is 40% higher, the spectral expansion is much more restricted in GeSe glass compared to TGG glass. These observations are related to the intrinsic properties of both materials. It is known that substituting Se atoms by heavier and more polarizable Te atoms increases the band-gap wavelength, shifts upward the IR transmission wavelength edge and increases both linear and non-linear refractive indices. The addition of fourfold coordinated Ge and threefold coordinated Ga mainly contributes to enhance the physicochemical properties of the glass (by raising T_g as well as enlarging the glass-forming range). Based on the aforementioned, compared with GeSe glass, TGG glass exhibits a transmission window more extended to the MIR region (Fig. 1b, c) and is expected to have higher non-linear properties. These properties will enhance the efficiency of the non-linear dynamics at the origin of the spectral broadening, allowing thus a better spectral enlargement despite the use of $\sim 2/3$ of the energy employed in the case of GeSe.

3.5 Impact of the detection setup on the MIR supercontinuum spanning

Figure 4 shows continuum and transmission spectra registered on GeSSe glass sample. In the present case, the decrease in the spectrum (hashed square) takes place in the range of maximum sensitivity of the MCT detector. Consequently, this phenomenon is mainly due to the oxide impurities present in the volume of the glass. However, the most interesting information concerns the intensity decrease pattern. This decrease pattern of the continuum is different than that of the transmission. Despite the loss of almost 30% of the transmission in the 7–10- μm range, the non-linear phenomena resist the impurities absorptions and the significant continuum decrease starts from $\sim 9.5 \mu\text{m}$. On the other hand, despite the steep decrease of transmission in the 10–11.5- μm region, mainly due to S–S two-phonon absorption, the continuum decreases progressively and reaches the noise level of the detection system around 10.8 μm , almost at mid-distance between the maximum around 10 μm and the minimum at 11.5 μm . These results confirm that the non-linear phenomena at the origin of the spectrum broadening can overcome the extrinsic absorptions. However, in the case of intrinsic absorptions, such as multiphonon, supercontinuum decrease takes place in the same way as the transmission.

Figure 5 shows continuum and transmission spectra registered on TGG glass sample. In this case, the decrease in intensity (hashed square) occurs in the lowest sensitivity range of the MCT detector. The continuum decrease is very steep in the 15–16- μm range. Knowing that this range exhibits a maximum transmission level and does not intersect with any extrinsic (impurities) or intrinsic (network) absorptions (Fig. 5), it is the steep decrease of the detector sensitivity that should account for the observed decrease in the registered supercontinuum intensity.

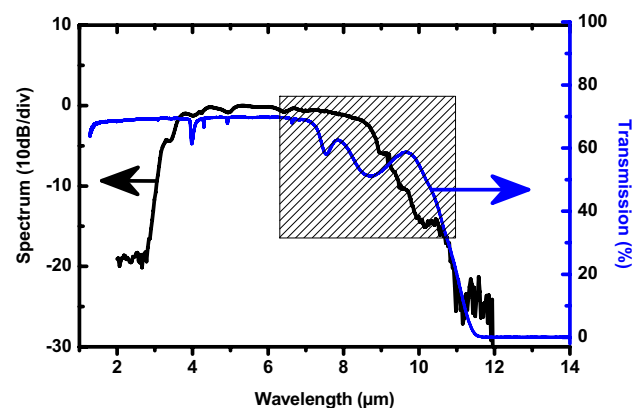


Fig. 4 Continuum and transmission spectra registered on GeSSe glass sample. Hashed square highlights the range where the signal decrease occurs

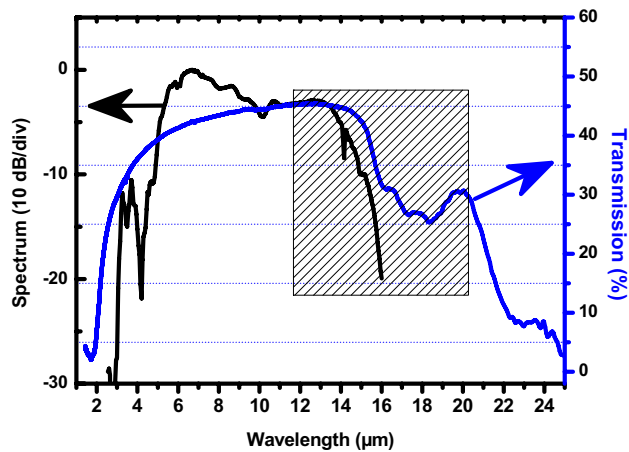


Fig. 5 Continuum and transmission spectra registered on TGG glass sample. Hashed square highlights the range where the signal decrease occurs

As we concluded above, non-linear phenomena at the origin of the supercontinuum generation can relatively resist and overcome the strong extrinsic absorptions, even at upon losing $\sim 30\%$ of the transmission (as clearly seen in Fig. 4). From Fig. 5, one could expect a supercontinuum extension above the MCT detection limit. Further work will consist now to first synthesis pure ChGs without unsuitable extrinsic absorption in the intrinsic transmission range of the glasses, and second to perform a new set of experiments with an extended detection range MCT detector.

4 Conclusion

We have demonstrated the generation of MIR supercontinuum pulses with several μJ pulse energies using three As- and Sb-free chalcogenide glasses [$\text{Ge}_{23.8}\text{S}_{57.1}\text{Se}_{19.1}$ (GeSSe), GeSe_4 (GeSe), and $\text{Te}_{75}\text{Ge}_{15}\text{Ga}_{10}$ (TGG)] and technologies already available in ultrafast optics. The supercontinuum spectra span more than 2 octaves in the 2.6–11-, 2.6–12-, and 2.5–16- μm ranges, respectively. The non-linear phenomena at the origin of the spectrum broadening can successively resist and overcome the remaining extrinsic absorptions. However, in the case of intrinsic absorptions, such as multiphonon, the supercontinuum decrease takes place in the same way as the transmission.

Acknowledgements We acknowledge the financial support from the Conseil Régional de Bourgogne and the FEDER (Fonds Européen de Développement Régional) through the Photcom PARI program. This project has been performed in cooperation with the Labex ACTION program (contract ANR-11-LABX-0001-01).

References

1. R.R. Alfano, S.L. Shapiro, Emission in the region 4000 to 7000 Å via four-photon coupling in glass. *Phys. Rev. Lett.* **24**, 584–587 (1970)
2. R. Osellame, G. Cerullo, R. Ramponi, *Femtosecond Laser Micromachining: Photonic and Microfluidic Devices in Transparent Materials* (Springer Science & Business Media, Berlin, 2012)
3. M. Durand, A. Houard, B. Prade, A. Mysyrowicz, A. Durécu, D. Fleury, B. Moreau, O. Vasseur, H. Borchert, K. Diener, R. Schmitt, F. Théberge, M. Chateaneuf, J. Dubois, Kilometer range filamentation: effects of filaments on transparent and non-transparent materials at long distances, in *CLEO:2011—Laser Applications to Photonic Applications*, OSA Technical Digest (CD) (Optical Society of America, 2011), paper CThFF3
4. S. Tzortzakis, L. Sudrie, M. Franco, B. Prade, A. Mysyrowicz, A. Couairon, L. Bergé, Self-guided propagation of ultrashort IR laser pulses in fused silica. *Phys. Rev. Lett.* **87**, 213902 (2001)
5. L. Bergé, S. Skupin, R. Nuter, J. Kasparian, J.-P. Wolf, Ultrashort filaments of light in weakly ionized, optically transparent media. *Rep. Prog. Phys.* **70**, 1633 (2007)
6. Y.E. Geints, A.A. Zemlyanov, Numerical simulations of ultrashort laser pulse multifilamentation in fused silica: plasma channels statistics. *J. Opt.* **18**, 015501 (2015)
7. V.Q. Nguyen, J.S. Sanghera, I.D. Aggarwal, I.K. Lloyd, Physical properties of chalcogenide and chalcogen halide glasses. *J. Am. Ceram. Soc.* **83**, 55–859 (2000)
8. S. Danto, P. Houizot, C. Boussard-Pledel, X.H. Zhang, F. Smektala, J. Lucas, A family of far-infrared-transmitting glasses in the Ga–Ge–Te system for space applications. *Adv. Funct. Mater.* **16**, 1847–1852 (2006)
9. E. Zhu, B. Wu, X. Zhao, J. Wang, C. Lin, X. Wang, X. Li, P. Tian, Surface crystallization behavior and physical properties of $(\text{GeTe}_4)_{85}(\text{AgI})_{15}$ chalcogenide glass. *Infrared Phys. Technol.* **86**, 135–138 (2017)
10. A. Zakery, S.R. Elliott, *Optical Nonlinearities in Chalcogenide Glasses and Their Applications* (Springer, Berlin, 2007)
11. B.J. Eggleton, B. Luther-Davies, K. Richardson, Chalcogenide photonics. *Nat. Photonics* **5**, 141–148 (2011)
12. J. Hu, J. Meyer, K. Richardson, L. Shah, Feature issue introduction: mid-IR photonic materials. *Opt. Mater. Express* **3**, 1571–1575 (2013)
13. L. Li, H. Lin, S. Qiao, Y. Zou, S. Danto, K. Richardson, J.D. Musgraves, N. Lu, J. Hu, Integrated flexible chalcogenide glass photonic devices. *Nat. Photonics* **8**, 643–649 (2014)
14. Z. Zhao, B. Wu, X. Wang, Z. Pan, Z. Liu, P. Zhang, X. Shen, Q. Nie, S. Dai, R.C. Wang, Mid-infrared supercontinuum covering 2.0–16 μm in a low-loss telluride single-mode fiber. *Laser Photonics Rev.* **11**, 1770023 (2017)
15. V.S. Shiryaev, M.F. Churbanov, Recent advances in preparation of high-purity chalcogenide glasses for mid-IR photonics. *J. Non-Cryst. Solids* **475**, 1–9 (2017)
16. V.S. Shiryaev, M.F. Churbanov, Preparation of high-purity chalcogenide glasses, in *Chalcogenide Glasses* (Elsevier, 2014)
17. O. Mouawad, *Infrared Supercontinuum Generation and Aging Challenges in Sulfur-Based Chalcogenide Glasses Suspended Core Highly Non Linear Optical Fibers* (Université de Bourgogne, Dijon, 2014)
18. M. Rozé, L. Calvez, J. Rollin, P. Gallais, J. Lonnoy, S. Ollivier, M. Guilloux-Viry, X.-H. Zhang, Optical properties of free arsenic and broadband infrared chalcogenide glass. *Appl. Phys. A* **98**, 97 (2009)
19. J. Troles, V. Shiryaev, M. Churbanov, P. Houizot, L. Brilland, F. Desevedavy, F. Charpentier, T. Pain, G. Sнопatin, J.L. Adam,

- GeSe₄ glass fibres with low optical losses in the mid-IR. *Opt. Mater.* **32**, 212–215 (2009)
20. Y.D. West, T. Schweizer, D.J. Brady, D.W. Hewak, Gallium lanthanum sulphide fibers for infrared transmission. *Fiber Integr. Opt.* **19**, 229–250 (2000)
 21. Y. Kawamoto, S. Tsuchihashi, Glass-forming regions and structure of glasses in the system Ge–S. *J. Am. Ceram. Soc.* **52**, 626–627 (1969)
 22. O. Mouawad, S. Kedenburg, T. Steinle, A. Steinmann, B. Kibler, F. Désévéday, G. Gadret, J.C. Jules, H. Giessen, F. Smektala, Experimental long-term survey of mid-infrared supercontinuum source based on As₂S₃ suspended-core fibers. *Appl. Phys. B* **122**, 177 (2016)
 23. I. Savelli, O. Mouawad, J. Fatome, B. Kibler, F. Désévéday, G. Gadret, J.C. Jules, P.Y. Bony, H. Kawashima, W. Gao, T. Kohoutek, T. Suzuki, Y. Ohishi, F. Smektala, Mid-infrared 2000-nm bandwidth supercontinuum generation in suspended-core microstructured Sulfide and Tellurite optical fibers. *Opt. Express* **20**, 27083–27093 (2012)
 24. S. Than Singh, T. Umesh Kumar, S. Ravindra Kumar, Rib waveguide in Ga–Sb–S chalcogenide glass for on-chip mid-IR supercontinuum sources: design and analysis. *J. Appl. Phys.* **122**, 053104 (2017)
 25. M.R. Karim, B.M.A. Rahman, Numerical investigation of mid-infrared supercontinuum generation in GeAsSe based chalcogenide photonic crystal fiber using low peak power. *Appl. Phys. Res.* **8**, 29–37 (2016)
 26. O. Mouawad, F. Amrani, B. Kibler, J. Picot-Clémente, C. Strutynski, J. Fatome, F. Désévéday, G. Gadret, J.C. Jules, O. Heintz, E. Lesniewska, F. Smektala, Impact of optical and structural aging in As₂S₃ microstructured optical fibers on mid-infrared supercontinuum generation. *Opt. Express* **22**, 23912–23919 (2014)
 27. Y. Yu, X. Gai, P. Ma, D.-Y. Choi, Z. Yang, R. Wang, S. Debbarma, S.J. Madden, B. Luther-Davies, A broadband, quasi-continuous, mid-infrared supercontinuum generated in a chalcogenide glass waveguide. *Laser Photonics Rev.* **8**, 792–798 (2014)
 28. M. Liao, W. Gao, T. Cheng, Z. Duan, X. Xue, H. Kawashima, T. Suzuki, Y. Ohishi, Ultrabroad supercontinuum generation through filamentation in tellurite glass. *Laser Phys. Lett.* **10**, 036002 (2013)
 29. A.A. Wilhelm, C. Boussard-Plédel, J.Q. Coulombier, B. Lucas, Bureau, P. Lucas, Development of far-infrared-transmitting Te based glasses suitable for carbon dioxide detection and space optics. *Adv. Mater.* **19**, 3796–3800 (2007)
 30. M. Liao, W. Gao, T. Cheng, X. Xue, Z. Duan, D. Deng, H. Kawashima, T. Suzuki, O. Yasutake, Five-octave-spanning supercontinuum generation in fluoride glass. *Appl. Phys. Express* **6**, 032503 (2013)
 31. V. Kokorina, *Glasses for Infrared Optics* (CRC Press, Boca Raton, 1996)
 32. R. Lin, F. Chen, X. Zhang, Y. Huang, B. Song, S. Dai, X. Zhang, W. Ji, Mid-infrared optical properties of chalcogenide glasses within tin-antimony-selenium ternary system. *Opt. Express* **25**, 25674–25688 (2016)
 33. S. Cui, C. Boussard-Plédel, J. Lucas, B. Bureau, Te-based glass fiber for far-infrared biochemical sensing up to 16 μm. *Opt. Express* **22**, 21253–21262 (2014)
 34. P. Lucas, B. Bureau, Selenide glass fibers for biochemical infrared sensing, in *Applications of Chalcogenides: S, Se, and Te*, ed. by G.K. Ahluwalia (Springer International Publishing, Cham, 2016), pp. 285–319
 35. L.G. Aio, A.M. Efimov, V.F. Kokorina, Refractive index of chalcogenide glasses over a wide range of compositions. *J. NonCryst. Solids* **27**, 299–307 (1978)
 36. S. Zhang, X. Zhang, M. Barillot, L. Calvez, C. Boussard, B. Bureau, J. Lucas, V. Kirschner, G. Parent, Purification of Te₇₅Ga₁₀Ge₁₅ glass for far infrared transmitting optics for space application. *Opt. Mater.* **32**, 1055–1059 (2010)
 37. Q. Guanshi, Y. Xin, K. Chihiro, L. Meisong, C. Chittrarekha, S. Takenobu, O. Yasutake, Ultrabroadband supercontinuum generation from ultraviolet to 6.28 μm in a fluoride fiber. *Appl. Phys. Lett.* **95**, 161103 (2009)
 38. J.H. Marburger, Self-focusing: theory. *Prog. Quantum Electron.* **4**, 35–110 (1975)
 39. O. Mouawad, P. Béjot, F. Billard, P. Mathey, B. Kibler, F. Désévéday, G. Gadret, J.C. Jules, O. Faucher, F. Smektala, Mid-infrared filamentation-induced supercontinuum in As–S and an As-free Ge–S counterpart chalcogenide glasses. *Appl. Phys. B* **121**, 433–438 (2016)